

A time-of-flight spectrometer for unslowed fission fragments

A.A. Alexandrov, I.A. Alexandrova, A.V. Ermolenko, Yu.A. Korjuk, D.S. Nikulin, Yu.F. Pevchev, S.L. Podshibyakin, Yu.V. Pyatkov, S.I. Sitnikov, A.I. Slyusarenko, A.N. Shemetov and R.A. Shehmametiiev

Moscow Engineering Physics Institute, 115409, Kashirskoye shosse, 31, Moscow, USSR

N.N. Demidovitch

All-Union Nonorganic Materials Research Institute, Moscow, USSR

Received 22 August 1990 and in revised form 24 January 1991

The one-armed time-of-flight spectrometer mounted in a vertical experimental port of the research reactor at the Moscow Engineering Physics Institute (MEPhI) was designed for measuring mass–energy distributions of unslowed fission fragments. The study of rare fission modes in the yield regions up to 10^{-6} is carried out having a target location near the reactor core and an electrostatic particle guide system installed, which increases the efficiency ratio of the spectrometer by a factor of 50. The special “heavy ion generator” operation mode of the spectrometer can be used for studies of fast (\sim MeV/amu) heavy ion interaction with matter. The fission fragment energy is measured by an ionization chamber or a semiconductor detector. The negligible angular divergence of the fragment beam enables fission fragment detection in a channeling registration mode to improve the energy resolution of semiconductor detectors. The fragment velocity is determined by the time of flight between two time pick-off microchannel plate detectors. A new procedure using unseparated fission fragments was developed to obtain the correct value for the time resolution of the system.

1. Introduction

A significant part of the information available on fission has been provided by the mass–energy–charge analysis of fission fragments (FF) distributions. The measurement of the mass and nuclear charge distributions for unslowed FF in correlation with their kinetic energy gives the possibility to study the dynamic aspects of the fission process when the compound nucleons system moves from the saddle point to scission.

In the last few years a great progress in the experimental technique was achieved by the time-of-flight method of FF mass determination combined with charge identification by the measurement of the specific energy loss or particle range in a high resolution ionization chamber. In the framework of this approach the best results were obtained with the “Cosi Fan Tutte” spectrometer mounted on the external neutron beam of a high-flux reactor in Grenoble [1].

However, at thermal flux intensities on the target 5×10^9 n cm⁻² s⁻¹, the relatively low efficiency ratio of the installation 2.3×10^{-6} does not allow the use of the “Cosi Fan Tutte” efficiently for studies of rare fission modes of actinides with low fissility. This restriction is inherent to the time-of-flight method as a rea-

sonable flight base is required. Moreover, the most interesting results were obtained at the “Cosi Fan Tutte” in the one-armed configuration as the neutron emission greatly reduces the installation efficiency in the coincidence mode. But in the case of one-armed measurement one can locate the target in the vicinity of the reactor core where the neutron flux is high and thus enhance the available statistics of the data.

This is the concept of a time-of-flight spectrometer presented here. The spectrometer is based on a vertical experimental port in a thermal column of the research MEPhI reactor. The spectrometer was designed as a multipurpose installation for measuring FF multidimensional energy–mass–charge spectra as well as for studies of heavy ion interaction with matter.

2. Spectrometer systems

2.1. FF beam forming system

The spectrometer design is outlined in fig. 1 [2]. Facing the reactor core center is the fissile target (1) located close to the bottom of the vertical evacuated beam tube (2) which is 7.3 m long with inner diameter

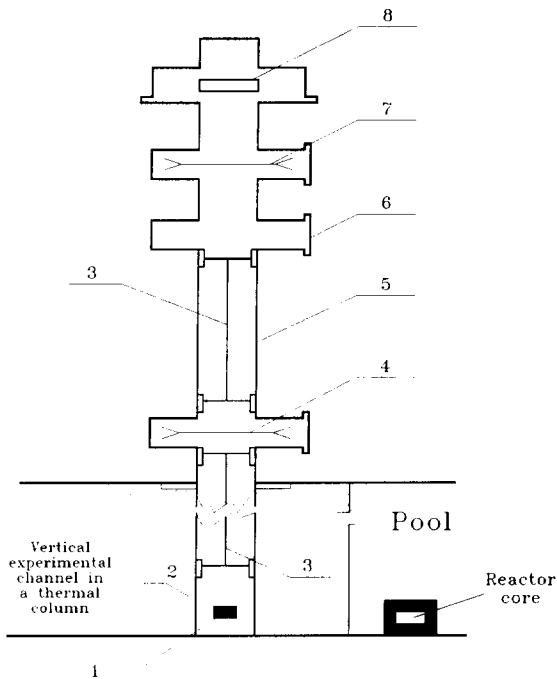


Fig. 1. General scheme of the spectrometer. For details see text.

of 23 mm. The built-in adjusting system provides the alignment of the tube with a sag not more than 2 mm. The thermal neutron flux at the target position is about $3.7 \times 10^{11} \text{ cm}^{-2} \text{ s}^{-1}$ with the cadmium ratio ≥ 400 .

The increase of the installation efficiency ratio compared with the geometrical one is achieved by an electrostatic particle guide system which is provided by a tubular coaxial capacitor formed by the tube wall and a thin metal electrode (3) stretched along its axis. When ions get into the capacitor electric field, a part of them is captured into the oscillation mode along the central electrode and in this manner they move in spiral paths along the guide system [3–5]. When the central electrode is at -2.5 kV potential to the tube wall, the installation efficiency ratio is 50 times the geometrical one and amounts to 1.5×10^{-6} .

The central electrode is fastened at the upper part of the guide system and is stretched under the weight of the target assembly. The target assembly design enables operation with the FF targets on a thin backing ($\sim 30 \mu\text{g cm}^{-2} \text{ Al}_2\text{O}_3$) without the protecting layer. These two factors are essential in determining the absolute FF kinetic energy values. The loss of the fissile material from the target because of the aggregate recoil does not exceed 16% during 100 h of operation. The change of the target thickness during the experiment is checked by the mean energies of the light and heavy FF groups. The FF beam forming system involves a specially selected collimators set, which enables the scattered FF

background to be suppressed by about two orders of magnitude. This design provides reasonable intensities for rare fission mode studies and adequate FF beam quality in the spectrometer detection system positioned on the upper reactor platform.

2.2. Detection system

The modulator spectrometer conception allows various detection systems to be realized. In the basic detection scheme the mass of fragment is obtained by FF time-of-flight of a predetermined distance between two microchannel plate time pick-off detectors (TPD) and their kinetic energy is measured in a total absorption detector – semiconductor detector (SCD) or gas ionization chamber. The start (4) and stop (7) TPDs used for measuring FF time-of-flight in the spectrometer are installed in separate evacuated detector chambers: between them there is a flight-path tube (5) and a detector chamber (6) for setting up the additional TPD when measuring the spectrometer time-path resolution by the method described below. The flight length in this detection scheme is 122 cm. To preserve the installation efficiency ratio the flight-path is also made in the form of a coaxial capacitor. At the end of the path length there is a vacuum chamber (8) with an SCD or a gas ionization chamber. The installation is evacuated up to 10^{-5} Torr by magnetodischarge and turbomolecular pumps.

2.2.1. Time pick-off detectors

For measuring FF time-of-flight of a fixed distance three different types of detectors were manufactured and tested. The general schemes of all detectors were taken from literature. The detectors differ by the method of secondary electron collection on the microchannel plates:

1) The assembly with the isochronous transfer of secondary electrons by 180° in a uniform magnetic field [6,7]. This TPD design allows for microchannel plates to be spaced out of the reactor experimental port radiation background. The permanent magnets were first applied in order to improve the stability of the detector.

2) The detector with secondary electrons moving in the axial electrical field [8,9]. The principal feature of this TPD type is the absence of an electron accelerating grid in the FF path which removes additional scattering of particles in the FF spectra measurements.

3) The device with secondary electron reflection by 90° by means of an electrostatic mirror [10,11]. This detector type permits one to determine the coordinate of the intersection point. A coordinate resolution of less than 1 mm was achieved.

The foils in TPD were made from colloid and formvar films $10 \mu\text{g cm}^{-2}$ thick with a $5\text{--}10 \mu\text{g cm}^{-2}$

one can hope to resolve neighboring masses even in the heavy FF group.

The necessary condition for channeling is a small beam angular divergence of the incoming ions, as the critical channeling angle does not exceed 1° . Under the specific conditions of this spectrometer the fraction of the channeling heavy FF group $^{235}\text{U}(n_{\text{th}}, f)$ is as great as 45% for surface barrier and 85% for ion-implanted detectors at zero potential on the central electrode of the particle guide system. At the particle guide system potential of more than 0.5 kV these values decrease by a factor of 1.6. The orientation of the detector is accomplished automatically following the method described in ref. [14]. The results of the channeling phenomena studies performed with this spectrometer are reported in refs. [15,16].

2.3. Spectrometer electronics and software

In developing the spectrometer data acquisition system [17] the main objective was given to decrease random signal superposition, which is highly important in investigations of rare fission modes. The scheme of the spectrometer system is presented in fig. 2. It involves two measuring circuits and a multilevel pulse selection system as well as the computer-based system for checking circuit parameters and stability control.

The spectrometer electronics is assembled from NIM and CAMAC modular blocks, while a PDP-11 analog microcomputer is used for acquisition and preliminary reduction of the incoming data. The spectra are recorded on the magnetic tape on an event-by-event basis. The signal selection is implemented on a logical level without analog processors to meet rigid requirements to the accuracy of the signal path characteristics.

The signals from TPDs enter the "start" and "stop" inputs of the time-amplitude converter (TAC) Ortec 467 via constant fraction discriminators (CFD) Ortec 473A. The TAC output pulse goes to the analog-to-digital converter ADC_1 (Schlumberger) via the dispersion amplifier (DA). In the normal operation mode the DA does not affect the incoming pulse. The signal from the energy detector passes the charge-sensitive preamplifier, the spectroscopy amplifier Ortec 572, the pulse expander Nokia LPA4848 and then enters the ADC_2 (Polon 712).

The event selection system includes the coincidence unit (CC) Polon 1402, a logic block (LB), the interrupt register Polon 303 and two single-channel analyzers Polon 1201 (SCA_1 and SCA_2). The coincident pulses from the logic outputs of the CFDs as well as the pulse from the preamplifier fast output with correspondingly adjusted delays determine uniquely the detected particle. The CC output is coupled via SCA_1 used as a controlled delay to the "enable" input of the TAC, thus performing a strobe signal. The other CC output in-

voke the program interrupt via the logic block and the interrupt register. The logic block acts as a linear gate. As the interrupt handling time in the microcomputer reaches 150 μs when the memory is being regenerated, the possibility of an overlap of pulses from two different particles may be about 10^{-4} , which is comparable with the rare fission modes yield. So the logic block is closed to prevent additional pulse pass until an LAM-signal is cleared by the program. Meanwhile, the second input of the interrupt register allows one to mark pile-ups in the energy circuit. These events are rejected when a pile-up is determined in the spectroscopy amplifier by the software.

Periodically the data acquisition is interrupted and the circuit calibration procedure is implemented. The Ortec 448 Research Pulser and Ortec 462 Time Calibrator are used to scan over the whole range of the energy and time circuits correspondingly. In this operation mode, the Gaussian noise is added to the time pulse by the DA to enhance the accuracy of peak determination. This procedure is fully automatic and uses program-controlled modules marked with arrows in fig. 2.

For reliable spectrometer operation the computer is provided with a special program-regenerator card [18] which restarts the computer in the case of random malfunctions in the program, hardware or the instrumentation leading to the interruption of data accumulation.

The spectrometer software was developed for a microcomputer-analog PDP-11 and solves the tasks of experiment simulating, data acquisition and archiving, experiment control, measuring circuit stabilization, data processing and representation. Data recording can be done either sequentially in the order of their arrival or in an integrated mode in the form of a matrix on the hard disc (for two-dimensional spectra up to 1024×1024 channels).

The data processing modules execute calibration correction procedures and mass-spectra evaluation algorithms. A computer code AUTOP [20] is used for peak parameter determination in one and two-dimensional spectra. The procedure includes the stages of peak search, deconvolution of multiplets and precision fitting of the spectrum by an analytical model function.

2.4. Heavy ions generator (HIG) mode

The spectrometer operation in the HIG mode provides an energetic ion beam with the predetermined mass and broad energy spectrum for detector researchers. The FFs knock out ions from a thin foil $\sim 1.5 \text{ mg cm}^{-2}$ located near the FF source by elastic scattering. A special target of 5 mg mass of fissile ^{235}U coating the inner surface of a cylinder [16] was made to optimize the relative yield of knocked-out ions. Fig. 3

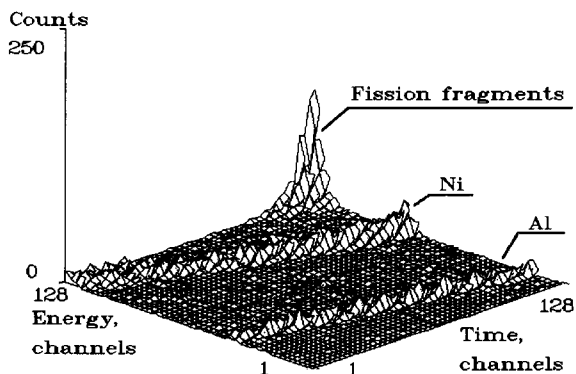


Fig. 3. Fragment of an “energy–time-of-flight” correlation spectrum in the “heavy ion generator” mode.

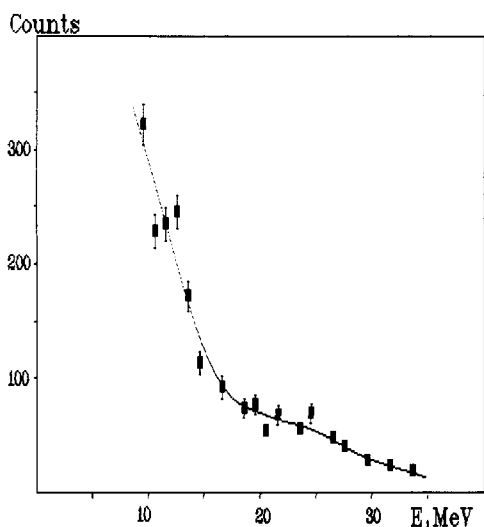


Fig. 4. Energy spectrum of detected Ni ions knocked out by fission fragments.

shows a fragment of a two-dimensional energy–time-of-flight spectrum of Al and Ni knocked-out ions measured in such a way of the spectrometer operation. The corresponding Ni-ion energy spectrum is shown in fig. 4. The characteristic ion flux level at the spectrometer detection system is 0.04 s^{-1} and 0.33 s^{-1} for Al and Ni, respectively.

3. Measurement procedure of the time-of-flight path resolution

Due to the lack of mass–energy separated FFs, the direct measurement of the spectrometer time-of-flight system resolution could not be realized under the experimental conditions presented here. The application of α -particles to this end presents some difficulties because of the low efficiency of α -particle registration in a TPD with formvar or colloid foils. Moreover, it is

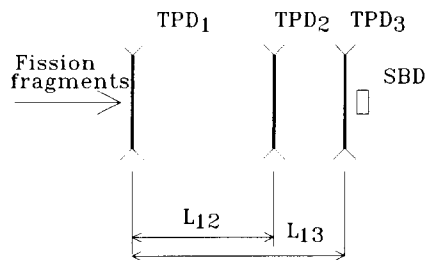


Fig. 5. Time calibration scheme: TPD is the time pick-off detector, L_{12} , L_{13} the flight bases, SBD the surface-barrier energy detector.

not quite legitimate to use α -particles as the dynamic range of the signal amplitudes in a TPD in this case differs significantly for α -particles and FF, due to greater number of secondary electrons knocked out from the foil by FFs. For this reason to measure spectrometer time-of-flight path resolution under real experimental conditions we have developed a method of correlated time-of-flight measuring with unseparated FFs. The method uses two flight bases with comparable length, one of which is the flight base of the spectrometer [21], and can be realized in the experiment presented schematically in fig. 5.

Here the TPD_1 provides the common start for two time-of-flight circuits with flight lengths L_{12} and L_{13} , while the stop signals are produced by the TPD_2 and TPD_3 , respectively. The result of this measurement is a correlation two-dimensional $N(X, Y)$ spectrum, where X and Y are the measured FF time of flight for L_{12} and L_{13} bases, correspondingly. The part of such an $N(X, Y)$ spectrum for $^{235}\text{U}(n_{th}, f)$ FF measured by the spectrometer is shown in fig. 6.

Let T be the true time-of-flight for the L_{13} base and KT for the L_{12} base, where $K = L_{12}/L_{13}$. Then one can define:

$$Y = T + t_3 - t_1,$$

$$X = K * T + t_2 - t_1, \tag{1}$$

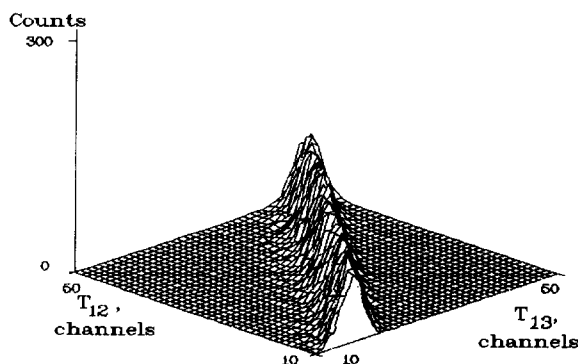


Fig. 6. Time correlation spectrum for $^{235}\text{U}(n_{th}, f)$ fission fragments.

where t_i , $i = 1-3$, is a random variable characterizing the operation uncertainty of the i th TPD. We assume t_i to be normally distributed with center 0 and dispersion τ_i^2 and independent of each other. On this basis the two-dimensional distribution density $P(X, Y)$ takes the form:

$$P(X, Y) = \int \Phi(T) \delta(Y - T - t_3 + t_1) \times \delta(X - KT - t_2 + t_1) dT, \quad (2)$$

where $\Phi(t_i)$ is given by the general FF time-of-flight distribution, and $\delta(Z)$ is a delta-function. In the slice at $Y = Y_0$ we have:

$$\begin{aligned} R(X) &= \int P(X, Y) \delta(Y - Y_0) dY \\ &= \int \Phi(T) \delta(Y_0 - T - t_3 + t_1) \\ &\quad \times \delta(X - KT - t_2 + t_1) dT \\ &= \Phi(Y_0 - t_3 + t_1) \\ &\quad \times \delta(X - KY_0 - Kt_3 - t_2 + (1 - K)t_1). \end{aligned} \quad (3)$$

Usually $|d\Phi/dT| \tau_i \ll \Phi$, so that $\Phi(Y_0 - t_3 + t_1) \approx \Phi(Y_0) = \text{const}$. In this case the eigenfunction of the distribution takes the form:

$$\begin{aligned} \hat{R}(q) &= \int_{-\infty}^{\infty} \exp(iqR(X)) dX \\ &= \exp(iq(KY_0 - Kt_3 + t_2 - (1 - K)t_1)), \end{aligned} \quad (4)$$

i.e. it is the product of separate exponents. It follows further that the distribution variance obtained in the slices of the $N(X, Y)$ -spectrum at a fixed Y is determined by:

$$Dx = K^2\tau_3^2 + \tau_2^2 + (1 - K)^2\tau_1^2. \quad (5)$$

Because τ_i is nothing but an intrinsic time resolution of the i th TPD, we can determine the time resolution of the spectrometer by measuring the width of the distribution in the slices of the correlation spectrum. If the flight lengths are approximately equal ($K \approx 1$), then:

$$\text{FWHM} \approx \gamma(\tau_2^2 + \tau_3^2)^{1/2}, \quad (\gamma = 2.35), \quad (6)$$

which corresponds to the resolution of the system of the two TPDs. Thus by interchanging the positions of TPD₂ for TPD₃ (this possibility is provided in the spectrometer design) and by using the TPD₃ as a start detector we can obtain the time-of-flight circuit with known time resolution.

If the time-of-flight paths are different in length, the TPD₂ and TPD₃ resolution can be determined according to two $N(X, Y)$ -spectra, with the only difference that TPD₂ and TPD₃ are interchanged. For a fixed

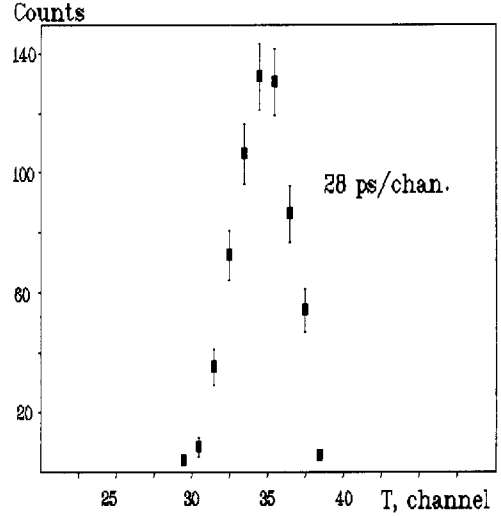


Fig. 7. Section of the time correlation spectrum at fixed value of $Y = 36$.

value of Y_0 a set of equations with respect to τ_2 and τ_3 can be obtained:

$$\begin{aligned} \text{FWHM}_1 &= \gamma(\tau_2^2 + K^2\tau_3^2)^{1/2}, \\ \text{FWHM}_2 &= \gamma(\tau_3^2 + K^2\tau_2^2)^{1/2}, \end{aligned} \quad (7)$$

from which these parameters are calculated.

The shift of the $N(X, Y)$ -spectra along the X -axis at such interchanges produces some difference in signal delays from the TPD₂ and TPD₃ which must be taken into account in obtaining the zero point of the spectrometer time scale.

The time-of-flight lengths L_{12} and L_{13} in the spectrometer are 99 and 122 cm, respectively. The spectrum presented in fig. 6 was measured by two TPDs with the secondary electrons transfer by 180° in a magnetic field. The channel cell value was 28 ps. One of the slices of the $N(X, Y)$ -spectrum at a fixed value $Y = 36$ is given in fig. 7. The FWHM of this distribution was 130 ± 5 ps.

The resolution (FWHM) of the two TPD systems calculated from the width of such $N(X, Y)$ -spectrum slices by eq. (5) was 160 ± 5 ps for the whole FF velocity range. Yet the contribution due to the TPD₂ foil energy loss spread by FFs with a fixed time-of-flight of L_{12} base with different nuclear charges has not been subtracted from this value. The value of this contribution in the spectrometer discussed is estimated to achieve ~ 30 ps. It should be noted that at the time-of-flight length $L_{12} \approx L_{13}$, the energy straggling in the TPD₂ foil does not affect the resolution definition by the method described above.

For the case when a TPD with the axial electric field was used as the TPD₂ we obtained the resolution depen-

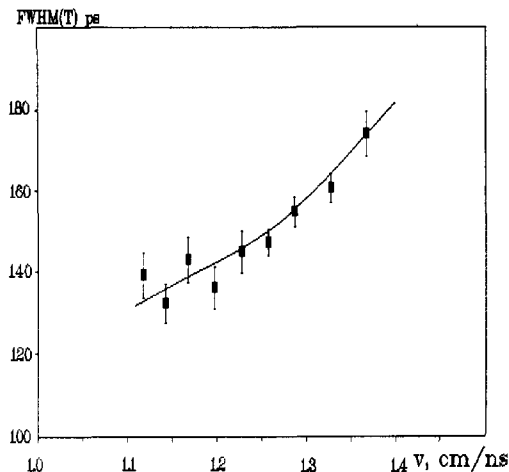


Fig. 8. Time resolution dependence vs. fragment velocity for the time pick-off detector with axial electric field.

dence on FF velocity, shown in fig. 8. Such a resolution degradation with the FF velocity increase could be explained by the signal amplitude contraction in this type of TPD, and hence, the reduction in signal-noise ratio is due to a smaller number of secondary electrons knocked out by faster FFs from the foil-emitter. The difference in signal delay from the two above-mentioned TPD types as determined by the $N(X, Y)$ -spectrum shift at the TPD₂ for TPD₃ interchange was 1.52 ns. Taking into account the spectrometer time-of-flight base length (122 cm) the relative resolution of the time-of-flight system as defined by the method described above is 0.1 and 0.2%, respectively for the heavy and light $^{235}\text{U}(n_{\text{th}}, f)$ FF groups.

4. Spectrometer calibration

The spectrometer time path calibration involves the definition of the time scale slope and zero point. The start and stop TPD being identical, the scale zero is determined by the self-coincidence peak position. For the case of nonidentical TPDs a correction for the inner signal delays from the TPDs is introduced by the above method. The time scale channel value is defined from the spectrum measured by means of the time calibrator Ortec 452. The necessary corrections due to the time scale nonlinearity are taken into account during the experimental spectra processing.

The special energy calibration is necessary because of the presence of the pulse-height defect. For semiconductor detectors the Shmitt calibration scheme [22] is usually performed. However, strictly speaking, this method is correct only for a special mark of detectors and the quality of calibration source manufacturing.

In this work we tried another method [23] based on the evaluation of mass spectra of unseparated FFs, which seems to be applicable for ionization chambers as well. The procedure in question seeks for the minimum difference between experimental mass spectrum and the known one (taken from compilations).

When an electrostatic particle guide system is used, an efficiency calibration is required for correct calculation of FF yields. This directly follows from the efficiency ratio ϵ dependence on the ionic charge q and E , the particle energy [3]:

$$\epsilon = 0.15 \frac{qU}{E \ln(R_2/R_1)}, \quad (8)$$

where U is the guide system voltage, R_1 and R_2 the inner and outer electrode radii of the guide system.

The evaluation of the efficiency correction factor is obtained by its parameterization as the FF velocity and energy function. The associated procedure involves measuring the two-dimensional energy-time-of-flight FF spectra at zero voltage on the central electrode of the particle guide system $R(X, Y)$ and with the operating voltage $S(X, Y)$. Here X is an energy code and Y a time-of-flight code. By parameterization of the $\epsilon(X, Y)$ relationship as $\epsilon = F(\mathbf{P}, X, Y)$, where F is chosen as, for example, a biquadratic form:

$$F(\mathbf{P}, X, Y) = P_0 + P_1X + P_2Y + P_3X^2 + P_4XY + P_5Y^2, \quad (9)$$

P_i coefficients are determined from functional minimization condition in the form:

$$\phi(\mathbf{P}) = \sum_{X,Y} w(X, Y) (R(X, Y) - F(\mathbf{P}, X, Y)S(X, Y))^2, \quad (10)$$

where $w(X, Y)$ are the proper weights defined by count dispersion in two-dimensional S and R spectra channels. As the number of counts in two-dimensional spectrum channel is, as a rule, not large, one should take into account the Poisson distribution of counting numbers while defining dispersion. For accurate approximation in measuring results processing the function $F(\mathbf{P}, X, Y)$ was chosen as the product of a cubic spline in Y - and a linear function in X -direction. The dependence of the correction factor vs $^{242\text{m}}\text{Am}(n_{\text{th}}, f)$ FF time-of-flight is shown in fig. 9.

5. Conclusion

The characteristics of the time-of-flight FF spectrometer developed are shown in table 1.

The fission product target location in the immediate vicinity of the reactor core in conjunction with the electrostatic particle guide system provided an im-

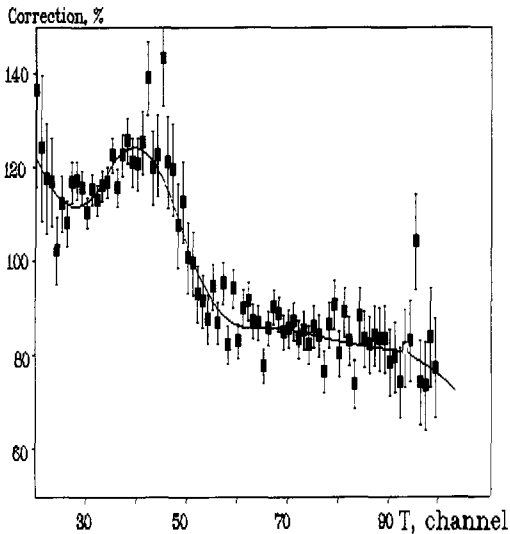


Fig. 9. Electrostatic particle guide correction factor $\epsilon(X = \text{const}, Y)$ for $^{242m}\text{Am}(n_{\text{th}}, f)$ fission fragments. The points denote the ratio $R(X, Y)/S(X, Y)$.

proved FF registration intensity (above ~ 50 times that of the spectrometer “Cosi Fan Tutte” [1]), which is fair enough for the rare fission modes to be studied. The characteristics of the developed FF detectors and measuring circuits as well as the periodic control of their stability enable long-term precision measurements of mass–energy FF distributions up to $\sim 10^{-6}$ yield level. The availability of a heavy ion beam in the HIG mode and the TPD resolution definition method realized in the spectrometer by the use of nonseparated FF beam enable the studies of FF detector characteristics under real experimental conditions.

The spectrometer systems, as well as the correctness of all calibration procedures used, were tested in experiments on measuring mass–energy $^{233,235}\text{U}(n_{\text{th}}, f)$ FF distributions. The mass spectrum of $^{235}\text{U}(n_{\text{th}}, f)$ FF for a fixed kinetic energy 110 MeV (the window width 1 MeV) is presented in fig. 10, along with the data of

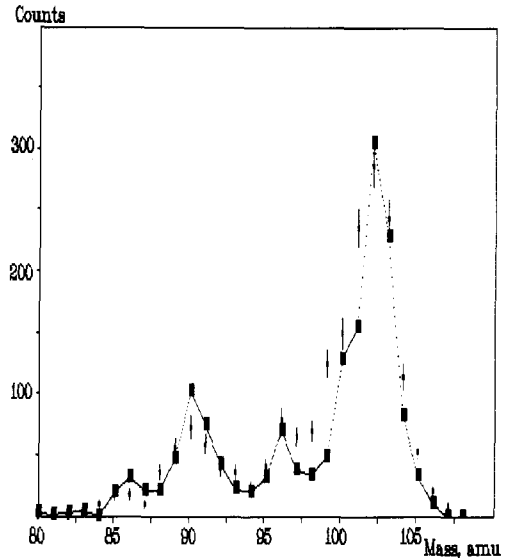


Fig. 10. Mass spectra of $^{235}\text{U}(n_{\text{th}}, f)$ fission fragments with fixed kinetic energy $E = 110$ MeV: \blacksquare denotes this work; \blacksquare ref. [24].

mass separator “Lohengrin” [24]. The agreement in position coincidence and relative intensities of mass peaks due to even–odd differences in the light FF group mass yields at 10^{-4} level is rather good. The mean kinetic energy dependence vs mass for the light group $^{235}\text{U}(n_{\text{th}}, f)$ FFs also agrees with the data of ref. [25] (fig. 11). In two-dimensional “mass–kinetic energy” spectra for $^{233,235}\text{U}(n_{\text{th}}, f)$ FFs a fine structure in the form of linear ridges has been noticed [26]. The full

Table 1
The spectrometer characteristics

Neutron flux density on the target	$3.7 \times 10^{11} \text{ n cm}^{-2} \text{ s}^{-1}$
Efficiency ratio	1.5×10^{-6}
Flight length	122 cm
Time resolution	160 ps
Mass resolution with SCD use	$\leq 2 \text{ amu}^a$
Ion flux intensity in the HIG	
mode: Al	0.04 s^{-1}
Ni	0.33 s^{-1}
Relative instability of measuring circuits	$< 0.2\%$

^a For the light FF $^{233}\text{U}(n_{\text{th}}, f)$ group.

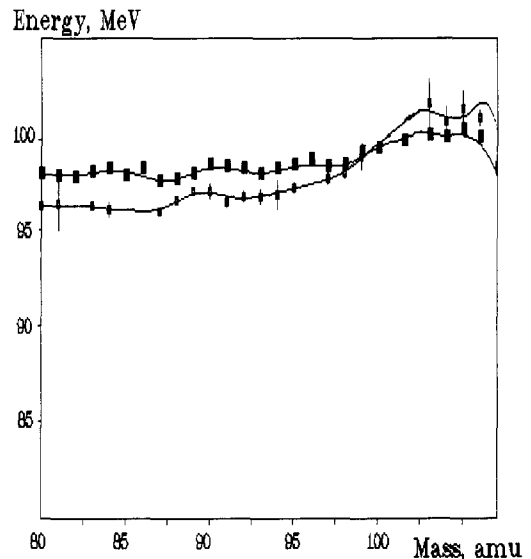


Fig. 11. Mean energy dependence vs mass for $^{235}\text{U}(n_{\text{th}}, f)$ fission fragments: \blacksquare denotes this work; \blacksquare ref. [25].

mass–energy distribution of $^{242m}\text{Am}(n_{\text{th}}, f)$ FFs including the cold fragmentation region [26] was measured in the spectrometer presented for the first time. This spectrometer may be a prototype of a two-armed installation at the high flux research reactor “PIK” of the Leningrad Nuclear Physics Institute.

References

- [1] A. Oed, P. Geltenbort, R. Brisso et al., Nucl. Instr. and Meth. 219 (1984) 569.
- [2] A.A. Alexandrov, N.N. Demidovich, Yu.F. Pevchev et al., Prib. tekhn. eksp. (USSR) 3 (1989) 38.
- [3] N.C. Oakey and P.D. McFarlane, Nucl. Instr. and Meth. 49 (1967) 220.
- [4] S.V. Ermakov, Yu.V. Pyatkov, A.I. Slyusarenko et al., in: Experimental Methods of Nuclear Physics in the Fission Processes and Products Researches, Moscow (1983) p. 25.
- [5] Yu.V. Pyatkov, I.V. Romanov, A.I. Slyusarenko et al., in: Experimental Methods of Nuclear Physics, Moscow (1985) p. 3.
- [6] A.M. Zebelman, W.G. Ceyer, K. Nalbach et al., Nucl. Instr. and Meth. 141 (1977) 439.
- [7] A.A. Alexandrov, N.G. Volkov, Yu.V. Pyatkov et al., Prib. tekhn. eksp. (USSR) 6 (1981) 21.
- [8] E. Weissenberger, W. Kast and F. Gonnenein, Nucl. Instr. and Meth. 163 (1979) 359.
- [9] A.V. Ermolenko, Yu.V. Pyatkov, A.V. Tron et al., Voprosy atomnoy nauki i tekhniki 3 (1988) 65.
- [10] F. Busch, W. Pfeffer, B. Kohlmeier et al., Nucl. Instr. and Meth. 171 (1980) 71.
- [11] S.L. Podshibyakin, Yu.V. Pyatkov, A.I. Slyusarenko et al., Prib. tekhn. eksp. (USSR) 6 (1988) 67.
- [12] A. Oed, P. Geltenbort, F. Gonnenein et al., Nucl. Instr. and Meth. 205 (1983) 455.
- [13] C.D. Moak, Y.W.T. Dabbs and W.W. Walker, Rev. Sci. Instr. 3 (1966) 1131.
- [14] A.A. Alexandrov, A.I. Skuratov and A.I. Slyusarenko, in: Automatization of Experimental Researches in Nuclear Physics Moscow (1987) p. 55.
- [15] A.A. Alexandrov, N.S. Medvedeva, Yu.V. Pyatkov et al., preprint MEPhI, 072 - 86 (1986).
- [16] A.A. Alexandrov, N.N. Demidovich, V.F. Kushniruk et al., preprint MEPhI, 062 - 89 (1989).
- [17] A.A. Alexandrov, Yu.A. Korzuk, A.N. Shemetov et al., Prib. tekhn. eksp. (USSR) 4 (1989) 44.
- [18] S.I. Sitnikov, Microprocessornye sredstva i sistemy 2 (1990) 90.
- [19] S.A. Kassirov, G.G. Kovshevny, A.A. Kotov et al., Nucl. Instr. and Meth. 119 (1974) 301.
- [20] A.K. Churakov, A.A. Byalko and N.G. Volkov, preprint JINR, P10-86-621, Dubna (1986).
- [21] A.A. Alexandrov, N.N. Demidovich, Yu.A. Korjuk et al., preprint MEPhI, 077-88 (1988).
- [22] H.W. Shmitt, W.E. Kiker and C.W. Williams, Phys. Rev. 137 (4B) (1965) 837.
- [23] A.I. Per'kov, Yu.V. Pyatkov and A.I. Slyusarenko, Experimental Methods of Nuclear Physics, Moscow (1985) p. 18.
- [24] H.G. Clerc, W. Lang, M. Mutterer et al., Nucl. Instr. and Meth. A452 (1986) 277.
- [25] W. Lang et al., Nucl. Phys. A345 (1980) 34.
- [26] A.A. Alexandrov, I.A. Alexandrova, Yu.V. Pyatkov et al., Abstr. Int. Conf. 50th Anniversary of Nuclear Fission, Leningrad, USSR (1989) p. 127.
- [27] A.A. Alexandrov, I.A. Alexandrova, S.L. Podshibyakin et al., Int. School-Seminar on Heavy Ions Physics, Dubna, USSR (1989) p. 46.